Journal of Polymers and the Environment (2021) 29:2609–2627
https://doi.org/10.1007/s10924-021-02069-7

ORIGINAL PAPER

Effect of TiC Nanoparticles Reinforcement in Coir Fiber Based Bio/Synthetic Epoxy Hybrid Composites: Mechanical and Thermal Characteristics

H. Mohit[1] · M. R. Sanjay[1] · Suchart Siengchin[1] · Anish Khan[2,3] · Hadi M. Marwani[2,3] · Hurija Dzudzevic-Cancar[4] · Abdullah M. Asiri[2,3]

Accepted: 16 January 2021 / Published online: 30 January 2021

Abstract

The present investigation was performed to study the effect of titanium carbide (TiC) nanoparticles and coir fiber as hybrid reinforcements on the physical, mechanical characteristics, and thermal stability of Coir fiber/TiC epoxy composites. The hand layup technique was applied for the fabrication of composites by reinforcing a fixed quantity of coir fiber (0, 5, and 10 wt%) and TiC nanoparticles (0, 5, and 10 wt%) in the proportion of bio-epoxy Sr 33 (100, 95, and 90 wt%) and synthetic epoxy (100, 95, and 90 wt%) resin. The cured specimen were subjected to flexural, tensile, impact, shore hardness, and chemical resistance tests. The fracture surface of the epoxy composites was investigated from a scanning electron microscope (SEM). From the outcomes, it was found that the reinforcement of coir fiber in epoxy polymer showed better than the neat polymer in most of the considered properties. The incorporation of TiC nanoparticles in coir fiber/epoxy composites exhibited some improvement in the mechanical characteristics (tensile strength by 4.99% and flexural strength from 115.05 to 124 MPa) and thermal stability (up to 402.71 °C) of the developed composites, which have a resistance under different loading conditions.

Keywords Bio-epoxy · Chemical resistance · Contact angle · Tensile strength

Introduction

In recent years, the various natural-based fibers such as hemp, sisal, jute, kenaf, and coir have earned noticeable consideration as a reinforcement material to polymers because of their benefits over the conventional synthetic fibers as lower weight, low cost, higher mechanical properties, renewability and biodegradable [1–4]. The plant cellulose fiber-based laminates have been studied for broad applications in different fields such as civil, automobiles, packaging, consumer goods, sports, and other structural engineering industries [5, 6]. Among the considerable plant cellulose fibers, coir is a versatile, renewable, biodegradable, abundant and low-cost lignocellulosic fiber obtained from the coconut tree (Cocos nucifera) fruit, which is broadly harvested in tropical zones [7, 8]. Also, the traditional utilization of coir fiber in-floor furnishing, cushion, cordage, ropes, carpets, etc. This natural based raw substance has exhibited a higher possibility in the field of bio-composite material because of many beneficial characteristics such as rigidity, elongation at break, resistance to weathering and

✉ M. R. Sanjay
mcemrs@gmail.com

Suchart Siengchin
suchart.s.pe@tggs-bangkok.org

Anish Khan
anishkhan97@gmail.com

[1] Natural Composites Research Group Lab, Department of Materials and Production Engineering, The Sirindhorn International Thai-German Graduate School of Engineering (TGGS), King Mongkut's University of Technology North Bangkok (KMUTNB), Bangsue, Bangkok 10800, Thailand

[2] Chemistry Department, Faculty of Science, King Abdulaziz University, Jeddah 21589, Saudi Arabia

[3] Center of Excellence for Advanced Materials Research, King Abdulaziz University, Jeddah 21589, Saudi Arabia

[4] Department of Natural Science in Pharmacy, Faculty of Pharmacy, University of Sarajevo, Zmaja od Bosne 8, 71 000 Sarajevo, Bosnia and Herzegovina

resilience [9–11]. The matrix is an essential component of the fiber-based composites due to it offers a shield against the adverse environments, defends the surface of the fiber from mechanical scrape/scratch, and transmits the load to the reinforced fibers. In general, matrices presently utilized in the plant cellulose fiber composites are polymers, which includes thermosets and thermoplastics. Even though the thermoplastic polymers have the benefit of efficiently recycled, higher mechanical characteristics are commonly attained with thermoset polymers such as polyester, vinyl ester, and epoxy resin [12]. The significant limitations of plant cellulose fibers as reinforcements in polymeric laminates are incompatible between the hydrophobic and hydrophilic behavior of matrix and cellulose fiber, respectively [13, 14]. These characteristics tend to poor matrix-cellulose fiber adhesion and inefficient mechanical performance as an outcome of the lower content of cellulose fiber and matrix load transmission [15].

To enhance the performance of coir fiber in epoxy composites further, some investigators applied synthetic fibers like Kevlar, aramid, and glass as peripheral reinforcement materials. It is observed that the mechanical characteristics of the fabricated coir hybrid epoxy composites with the reinforcement of Kevlar fiber, and glass fiber was improved by 5.15, and 2.67 times respectively when compared with the coir fiber epoxy composites [16–18]. Nonetheless the synthetic/coir fiber hybrid laminates provided higher characteristics, they also have certain issues like decrement in bio-degradability and increment in cost of fabrication for the hybrid laminates [19]. To overcome this problem, the coir fiber based hybrid laminates were developed with some well-established plant fibers such as luffa fiber (tensile strength of 29.67 MPa, flexural strength of 110.55 MPa, impact strength of 7.5 kJ/m^2) [20], sisal fiber (tensile strength of 371.18 MPa, flexural strength of 80.98 MPa and impact strength of 27.43 kJ/m^2) [21], and palmyra palm fibers (tensile strength of 40.31 MPa, compression strength of 45.8 MPa, flexural strength of 118.21 MPa, and impact strength of 48.2 kJ/m^2) [18] and improved the mechanical characteristics of the epoxy hybrid composites. Rahman et al. [9] investigated the effect of coir fiber reinforcement in polymethacrylate matrix and found that there is a significant improvement in the tensile properties (tensile strength up to 160 MPa) with the 20% of alkaline treatment followed by the grafting process modified with 50% of ethylene dimethylacrylate under lower effect of Ultra-violet radiation. Zhang and Hu [11] the combination of rice straws and coir fibers have been utilized as a potential reinforcement for particleboard composites and found that the increment of coir fiber improved the bonding strength by 365.85% and reduced the tensile strength by 40.34% and also observed as 40 vol% of fiber content as an optimal condition.

The incorporation of particles has become an essential technique to enhance the characteristics of composite materials. Presently, nanofillers have been broadly utilized in polymers, ceramics, and metals, etc. [22–24]. While comparing with traditional micro-particles, the mechanical characteristics of nanofiller reinforced polymer composites are significantly enhanced because of the larger surface area. For fiber-reinforced polymer composites (FRPCs), nanofiller (metal, carbon, mineral, and ceramic-based) can be utilized to enhance the fatigue resistance, delamination of FRPCs, fracture toughness, impact energy and interlaminar shear strength [25]. Also, in particle reinforced polymer composites; nanofillers have been actively used in various fields such as surface coatings, cold spray, microfluidics, etc. [26–28]. Presently, broad investigations have been performed to determine the mechanical characteristics of particle incorporated polymer composites. Li et al. have produced polyimide/silica zeolite blend, polyimide/functionalized silica zeolite composite, and polyimide films by irregular copolymer condensation process. The outcomes exhibit that the functionalized composite film presents the better toughened and reinforced characteristics, which substantially decrements the dielectric constant and improves the efficiency of protection from ultra-violet radiation [29]. Feng et al. have investigated the general electro-mechanical characteristics of nanofiller reinforced polymer laminate with a uniform distribution of nanofillers within the matrix [30]. Rianyoi et al. have produced piezoelectric ceramic reinforced Portland cement composite materials without using lead and mixed barium titanate particles under different concentrations and sizes. The outcomes exhibited that electromechanical characteristics are improved with incrementing the particle size [31]. Nam et al. have illuminated a hasty technique to enhance the thermo-mechanical features and electrical conductivity of silver nanowire reinforced polymer-based composites by strengthening silica nanofillers within the matrix. The outcomes signify that an electrical network can be produced at a lower volume proportion of silver nanofiller [32].

Recently, many scientists have introduced different types of nanoparticles as an additive or filler to enhance the thermal and mechanical features of the fiber reinforced polymer composites. Pathak et al. investigated the electrical and thermo-mechanical characteristics of reduced graphene oxide incorporated polyaniline-dodecylbenzene sulfonic acid-based polymer nanocomposites and found that the reinforcement of 0.3 wt% of reduced graphene oxide enhanced electrical, interfacial, and thermo-mechanical characteristics of polymer nanocomposites [33]. Hence, plant cellulose fiber hybridization with nanoparticles has currently shown an interest in attaining higher mechanical components. It has been noted that the addition of a very lower percentage of nanoparticles significantly enhances the structural properties of cellulose fiber-reinforced polymer laminates

[34–36]. Seretis et al. studied the effect of sonication on graphene/glass fiber reinforced epoxy polymer nanocomposites for mechanical characteristics and found that the increment in sonication time improved the tensile properties and decreased the flexural strength of polymer composites [37]. Pathak et al. investigated that the addition of graphene oxide till 0.3 wt% in carbon-based epoxy composites improved the shear and flexural strength, and followed a backtrack trend under higher concentration of graphene oxide [38, 39].

The desired characteristics of polymer composite is attained by reinforcing two or more nanofillers in the matrix. Presently, the researchers are focusing on a new kind of nanofillers to produce high performance polymer composites. Apart from these, ceramic materials are an efficient solution to offer the superior characteristics to polymer composites, due to their unique features than traditional nanofillers. Ceramic materials are well established in the field of composite materials due to they can be utilized in different applications such as semiconductors, batteries, transducer, and any other mechatronic devices [40–42]. Among the different types of ceramic materials, titanium carbide (TiC) is a well-established ceramic filler material for metal and polymer based composites because of a higher melting point, relatively lower coefficient of thermal expansion, higher elastic modulus and wear resistance [43–46]. Composite schemes containing a polymer resin and conductive particulates of TiC have been employed as a new division of engineering materials, due to its capability to move from negative to positive temperature conductivity coefficient [47]. These particles are presently applied as reinforcement material to any metals or alloys for producing thermally stable material to withstand at enormous temperature because of its melting point of 3065 ºC [48]. Dogan et al. fabricated steel and nickel-based composites with higher wear resistance by adding a lower volume of TiC particles, and found improvement in mechanical and tribological characteristics [49]. The epoxy polymer reinforced with nitrogen-doped graphene and TiC particles for high-performance absorbers production and found that it can be applicable for electromagnetic and dielectric applications [50]. El-Tantawy investigates the TiC micro-particles reinforced EPDM (ethylene-propylene-diene monomer) and found that there is an improvement in the thermal conductivity of the composites significantly under the higher loading of TiC filler [51].

Moreover, significant interest has not been observed on the physical characteristics of the polymer composites reinforced with TiC nanoparticles [51]. Nevertheless, the TiC has been found to enhance the properties of fiber-reinforced polymer composites, but there is no previous investigation on developing coir fiber reinforced epoxy polymer laminates with TiC as filler material. The overall TiC market is increasing because of various processing methods, the comfort of processing, lower cost, and a broad area of applications. Also, a lower concentration of TiC is sufficient for the transformation of polymer-based nanocomposites.

With the increasing demand for TiC particles in different applications, TiC is forecasted to be applicable at a cheaper rate in the upcoming future. Considering the enhancement in materials' characteristics because of reinforcement of TiC nanoparticles, in the current work, the influence of the same on coir-based polymer composites is beneficial. The objective of this present investigation is to examine the impact of TiC nanoparticles on the physical, mechanical, and thermal characteristics of epoxy laminates reinforced by coir fiber. TiC/coir/bio epoxy Sr 33 and TiC/coir/synthetic epoxy composites are fabricated using a hand layup technique. To study the impact of TiC nanoparticles on coir/bio and coir/synthetic epoxy composites, mechanical property tests such as flexural, tensile, impact, and hardness along with porosity, density, water absorption, chemical resistance, contact angle, and thermal stability are conducted.

Materials and Methods

Materials

In this present investigation, two types of epoxy resins have been utilized, such as Bio epoxy Sr 33 (GreenPoxy, (GP33) with Surf Clear ultra-slow hardener SD 4990) and synthetic epoxy Epotec YD-535 LV were utilized as a matrix. From the manufacturer's data, the viscosity of bio epoxy Sr 33 resin and hardener SD 4990 are 410–6380 mPa s and 8–25 mPa s respectively, and the density of bio epoxy Sr 33 and hardener SD 4990 is 1.159 g/cm^3 and 0.95 g/cm^3, respectively, produced by Sicomin epoxy systems, France and procured from Alpha Composition International Co. Ltd., Thailand. Synthetic epoxy resin YD-535 LV, semi-solid viscous materials, with a viscosity of 1235 cP and hardener of Epotec TH-725 with 10–20 cP are applied as a matrix in the present investigation, obtained from Aditya Birla Chemicals (Thailand) Limited. The coir fibers supplied from Tongmongkol Coconut fiber, Prachuapkhirikhan, Thailand, was utilized as a reinforcement for the fabrication of bio epoxy and synthetic epoxy composites. The nanofiller, i.e., TiC, was purchased from Zhuzhou Sanyinghe International Trade Co., Ltd., China, with a particle size of 10 nm also utilized as secondary reinforcement material.

Fabrication of Epoxy Composites

Processing of Coir Fibers

The coir fibers were washed and cleaned with flowing water to discard the dirt particle and then dried in sunlight for 3 days to remove the residual moisture content. The coir fibers are sectioned in small pieces, then transferred to Universal cutting mill, Pulverisette 19, FRITSCH, to convert the fibers into micro-particles. The obtained milled coir micro-fibers were further handled by sieving to collect the particle size less than 250 µm.

Development of Composite Material

The resin, hardener matrix, and the reinforcement elements were weighed into different weight fractions with the help of a digital weighing device. The specimen for the coir fiber and TiC nanoparticles/bio epoxy Sr 33 (BE33) and synthetic epoxy (SE) were weighed for each condition, as shown in Table 1. Similar steps were followed for synthetic epoxy composites separately.

Blending of the Components

The manual mixing of the components was applied to achieve a homogeneous distribution of particles within the polymer matrix. The coir micro-fibers and the TiC nanoparticles were combined with the hardener and epoxy, which was efficiently stirred with the help of a glass rod for 10 min to achieve the homogeneous dispersion. The combined mixture was immediately transferred into the die mold to avoid premature curing and permitted to vacate for ultra-slow curing time. Then, the fabricated samples were removed from the die mold and transferred to the heating furnace for 80 ± 2 °C for 24 h to remove the residual moisture content.

Characterization of Epoxy Composites

Physical Properties

The actual density of both bio epoxy Sr 33 and synthetic epoxy was determined by soaking weight method according to the ASTM D 792 standard test for the density of plastics and specific gravity from the Eq. (1).

$$\rho_{act} = \frac{W_{comp}}{W_{icomp} - W_{comp}} \tag{1}$$

where ρ_{act} is the actual density of the fabricated epoxy composite material, W_{icomp} is the weight after soaking in water and W_{comp} is the actual weight of the fabricated epoxy composite

The theoretical density of bio epoxy Sr 33 and synthetic epoxy can be achieved from Eq. (2).

$$\rho_{theo} = \frac{1}{\left(\frac{W_{fi}}{\rho_{fi}}\right) + \left(\frac{W_P}{\rho_P}\right)} \tag{2}$$

where ρ_{theo} is the theoretical density of epoxy composite, W_{fi} is the weight fraction of coir micro-fiber/TiC nanoparticles, W_P is the weight fraction of polymer (bio epoxy Sr 33 or synthetic epoxy), ρ_{fi} is the density of coir micro-fiber/TiC nanoparticles, ρ_P is the density of polymer (bio epoxy Sr 33 or synthetic epoxy). The difference between the actual and theoretical density of epoxy composite signifies the content of void as per the ASTM D 2734 standard. Hence, the void fraction (V_f) of the epoxy composite can be calculated from the Eq. (3). Five samples were experimented for the verifying the reproducibility of the outcomes.

$$V_f = \frac{\rho_{theo} - \rho_{act}}{\rho_{theo}} \tag{3}$$

The epoxy composites were sectioned and employed in glass slit, with a curing technique under 120 °C for

Table 1 Bioepoxy Sr33 and synthetic epoxy fabricated samples

Composite type	Description	Coir fiber	TiC Nanoparticles
BE33	Pure Bio-epoxy Sr 33 (GreenPoxy GP33 with Surf Clear ultra-slow hardener SD 4990)	–	–
CBE33	GreenPoxy GP33 Reinforced with coir fiber	10 wt%	–
ABE33	GreenPoxy GP33 Reinforced with TiC Nanoparticles	–	10 wt%
CABE33	GreenPoxy GP33 Reinforced with both coir fiber and TiC Nanoparticles	5 wt%	5 wt%
SE	Pure synthetic epoxy (Epotec kind) YD-535 LV with Epotec TH-725	–	–
CSE	Epotec YD-535 LV Reinforced with coir fiber	10 wt%	–
ASE	Epotec YD-535 LV Reinforced with TiC Nanoparticles	–	10 wt%
CASE	Epotec YD-535 LV Reinforced with both coir fiber and TiC Nanoparticles	5 wt%	5 wt%

600 seconds. The polishing procedures were conducted as per the sequence: 240, 400, 600 grit emery sheet. After the preparation of the surface, the fabricated epoxy composites were examined with polarized optical microscope HRM-300 from HUVITZ. The microscopic image examination was performed in the cross-sectional area of the fabricated epoxy composites, with 200x magnification and images were collected from DP 70 camera system. Finally, the images were examined using ImageJ software, and the mean value of porosity was determined from processed micrographs, which is utilized as an equivalent to the distribution of pore size and volume fraction of void content.

Five samples of 15 mm square were sectioned for water absorption test as per the ASTM D 570 standard from the fabricated epoxy composites. After the post-curing, the specimen was cooled over silica gel granules in desiccators before the water absorption was measured. The water absorption test was performed by immersing the sectioned samples in deionized water for 45 days and determined the weight increment when compared with the original weight after the post-curing of the sample. The test was conducted at room temperature of 24 ± 2 °C and 60% Relative humidity. Eq. (4) has been used for estimating the water absorption capacity of fabricated epoxy composites is shown below:

$$WA = \frac{W_2 - W_1}{W_1} \tag{4}$$

where W_1 is the weight of the sample before soaking and W_2 is the weight of the sample after 45 days of soaking in distilled water

Contact angle measurements of epoxy composites were determined with optical contact angle (OCA) 15 LJ data physics under room temperature (28 ± 2 °C and 60 ± 2%). For contact angle investigation, 1 µL of distilled water was poured on the sample surface using a glass syringe. The left and right side of the contact angle measurements were reported after equilibrium. For every specimen, the mean value of five readings was recorded as an outcome.

Mechanical Properties

The tensile test was conducted to measure the tensile stress of the epoxy-based polymer composites reinforced with either coir fibers or TiC nanoparticles and both. The samples were produced in a rectangular shape, in dimensions (100 (length) x 20 (width) x 3 (thickness) mm) and gauge length, as per the ASTM D 3039 standard. The test was conducted with a crosshead speed of 1 mm/min until fracture.

The flexural test specimen was produced according to the ASTM D 790 standard under a three-point bending test in Universal Testing Machine. The deflection of the epoxy polymer composites estimated under the compressive force until the sample cracks or breaks. The flexural force and displacement determined from the UTM for all the test specimens.

In every condition, tests were repeated five times, and the mean quantity was considered. The tests distributed with room temperature and relative humidity of 28 ± 2 °C and 60 ± 2%, respectively. The dimension of the epoxy samples for this test was 80 (length) x 15 (width) x 3 (thickness) mm.

The impact strength of epoxy polymer composites is its capability to absorption of energy from the impact force in the appearance of a smooth surface that focuses on the stresses. The Izod impact experiment was conducted according to the ASTM D 256 standard, with a dimension of 62.5 (length) x 12.5 (width) x 3 (thickness) mm.

The shore hardness of the epoxy-based polymer composites with coir fiber or TiC nanoparticles or both were experimented using Shore D indenter hardness testing machine. The indenter was pressured on the surface of composite samples till the bottom surface of the indenter is in complete contact with the composite. The dial gauge on the hardness testing machine signifies the value of the hardness of the composites. The same specimen was conducted under ten different locations of the composite specimen, and the mean hardness outcomes were measured. All the mechanical experiments were conducted in five replicates.

Fracture

Fracture examination of damaged samples was conducted from a tabletop scanning electron microscope in an FEI Quanta 450, operated with a higher vacuum medium under a secondary electron of 15 kV.

Fourier Transform infrared (FTIR) Spectra

FTIR was utilized to examine the epoxy composites with and without reinforcements of coir fiber or TiC nanoparticles or both particles, and a Perkin Elmer Spectrum 2, FTIR spectrometer was applied to determine the functional groups of both bio epoxy and synthetic epoxy composites, and the chemical bonds developed between the coir fiber or TiC nanoparticles or both and epoxy polymer. The tested specimen was converted into fine powders using a drilling machine and comprised with potassium bromide (KBr), then compressed into die with 10 mm of diameter under 70 MPa before the experimentation process. The wavenumber was ranged between 4000 and 400 cm^{-1} with a resolution of 1 cm^{-1}.

Thermal Characteristics

Thermogravimetric analysis (TGA) investigation was performed for epoxy polymer composites (5 (length) x 5 (width) x 3 (thickness) mm) incorporated with either coir fiber or TiC nanoparticles or both with the heating rate of 15 °C/min in the nitrogen atmosphere using TGA 2, Mettler Toledo, TGA/DSC 3 + HT/1600, Switzerland. The thermal decomposition of all samples appeared in a temperature range between 30 and 700 °C, and the weight loss performed and examined to measure the thermal characteristics. TGA also consists of degradation around 300 °C, and residual carbon content was observed at 600 °C from derivative thermograms (DTG).

Chemical Resistance Characteristics

The chemical resistance tests were performed by immersing the sample for 15 days under room temperature. The fabricated epoxy samples were positioned into different plastic cylindrical containers with alkali (10 wt% of NaOH), acid (30 wt% of H_2SO_4), and NaCl (10 wt%). Visual observations were performed for deterioration, softening, or damage like cracks, spoil, or blisters.

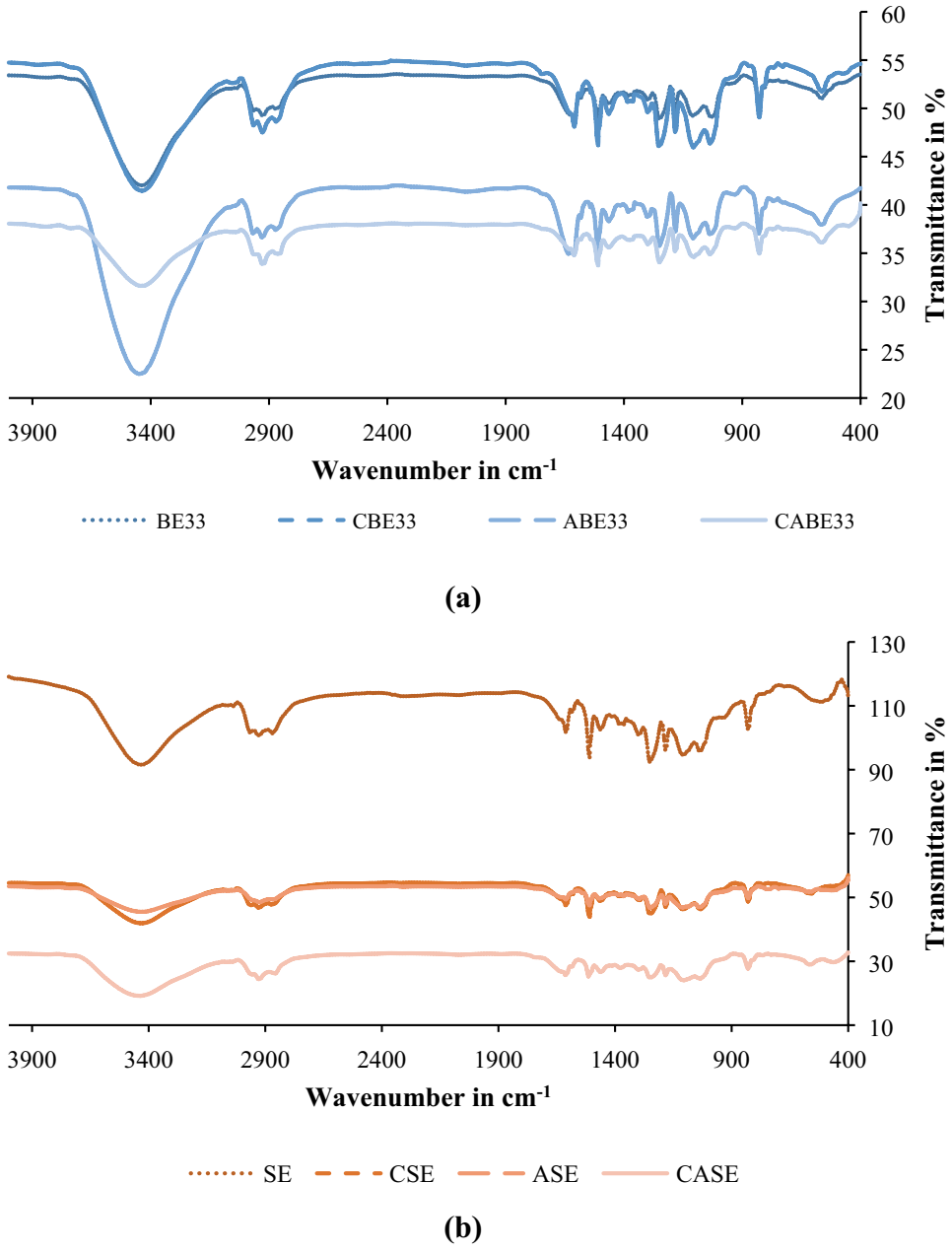

Fig. 1 FTIR spectra of coir fiber/TiC reinforced epoxy composites. **a** Bio-Epoxy 33 and **b** Synthetic epoxy composites

Results and Discussion

Effect on FTIR Spectra

Figure 1a and b shows the FTIR spectra of bio and synthetic epoxy polymer composites, respectively. The major wavenumber bands established in Fig. 1a are 3438.44, 3444.56, 3444.88, and 3438.42 cm^{-1} for BE33, CBE33, ABE33, and CABE33 respectively, whereas Fig. 1b are 3437.43, 3427.97, 3434, and 3435.19 cm^{-1} for SE, CSE, ASE, and CASE respectively indicated to Si–OH stretching of hydroxyl groups or moisture [52]. The various bands such as 2926.24, 2926.55, 2925.31, 2926.33, 2926.95, and 2924.75 cm^{-1} for BE33, CBE33, CABE33, SE, CSE, and CASE respectively for OH groups of cellulose, whereas these wavenumbers are absent in ABE33 and ASE [53]. Bands 1298 cm^{-1}, 1249.84–1107.23 cm^{-1}, 1032–1036 cm^{-1}, and 1584–1581 cm^{-1} are designated to C–O aromatic, C–O aliphatic, C–O alcoholic, and C=O stretching respectively as shown in the table in 2 and 3 for bio epoxy and synthetic epoxy composites. C=O is absent in BE33, ABE33,

Table 2 Assignment of FTIR spectrum of coir fiber/TiC reinforced bio epoxy 33 hybrid composites

Assignment	BE33	CBE33	ABE33	CABE33
Si–OH stretching	3438.44 cm^{-1}	3444.56 cm^{-1}	3444.88 cm^{-1}	3438.42 cm^{-1}
O–H stretching	2926.24 cm^{-1}	2926.55 cm^{-1}	Absent	2925.31 cm^{-1}
C=C stretching	1610.86 cm^{-1}	1609.95 cm^{-1}	1611.29 cm^{-1}	1609.48 cm^{-1}
NO_2 asymmetric stretching	1509.13 cm^{-1}	1509.14 cm^{-1}	Absent	1509.15 cm^{-1}
N–H stretching	1459.13 cm^{-1}	1459.12 cm^{-1}	Absent	1459.19 cm^{-1}
C–H bending	1382.7 cm^{-1}	1382.58 cm^{-1}	Absent	1376.52 cm^{-1}
C–O Aromatic stretching	1298.3 cm^{-1}	1297.37, 1250.51 cm^{-1}	1298.49 cm^{-1}	1297.58 cm^{-1}
C–O aliphatic stretching	1249.84, 1182.17, 1107.23 cm^{-1}	1182.13, 1106.16 cm^{-1}	1249.83, 1182.24, 1106.68 cm^{-1}	1249.9, 1182.15, 1106.83 cm^{-1}
C–O alcoholic stretching	1032.41 cm^{-1}	1036.31 cm^{-1}	1036.21 cm^{-1}	Absent
C–H out of plane bending	828.7 cm^{-1}	827.31 cm^{-1}	828.8, 766.61 cm^{-1}	827.92 cm^{-1}
C–H asymmetric stretching	Absent	2869.05 cm^{-1}	Absent	2855.74 cm^{-1}
C–H symmetric stretching	Absent	2964.46 cm^{-1}	Absent	Absent
C=O stretching	Absent	1583.02 cm^{-1}	Absent	Absent
N–H bending	Absent	1541.79 cm^{-1}	1551.5	Absent

Table 3 Assignment of FTIR spectrum of coir fiber/TiC reinforced synthetic epoxy hybrid composites

Assignment	SE	CSE	ASE	CASE
Si–OH stretching	3437.43 cm^{-1}	3427.97 cm^{-1}	3434 cm^{-1}	3435.19 cm^{-1}
O–H stretching	3037.45, 2926.33 cm^{-1}	2926.95 cm^{-1}	Absent	2924.75 cm^{-1}
C=C stretching	1609.59 cm^{-1}	1609.35 cm^{-1}	1609.09 cm^{-1}	1610.02 cm^{-1}
NO_2 asymmetric stretching	1509.16 cm^{-1}	1509.16 cm^{-1}	Absent	1509.18 cm^{-1}
N–H stretching	1462.84, 1455.91 cm^{-1}	1459.17 cm^{-1}	Absent	1459.18 cm^{-1}
C–H bending	Absent	1382.54 cm^{-1}	Absent	1382.31 cm^{-1}
C–O aromatic stretching	1297.57 cm^{-1}	1297.76 cm^{-1}	1298.08 cm^{-1}	1297.19 cm^{-1}
C–O aliphatic stretching	1249.75, 1182.24, 1106.14 cm^{-1}	1249.67, 1182.22, 1106.91 cm^{-1}	1249.03, 1182.94, 1107.04 cm^{-1}	1249.87, 1182.09, 1106.56 cm^{-1}
C–O alcoholic stretching	1037.69 cm^{-1}	1036.49 cm^{-1}	1037.64 cm^{-1}	1037.36 cm^{-1}
C–H out of plane bending	963.45, 827.81, 767.76 cm^{-1}	828.49, 766.42 cm^{-1}	829.19, 737.13 cm^{-1}	828.21 cm^{-1}
C–H asymmetric stretching	Absent	2870.12 cm^{-1}	Absent	2855.59 cm^{-1}
C–H symmetric stretching	2964.29 cm^{-1}	2964.46 cm^{-1}	Absent	Absent
C=O stretching	1581.97 cm^{-1}	1582.56 cm^{-1}	Absent	1582.81 cm^{-1}
N–H bending	Absent	1541.99 cm^{-1}	Absent	1541.98 cm^{-1}

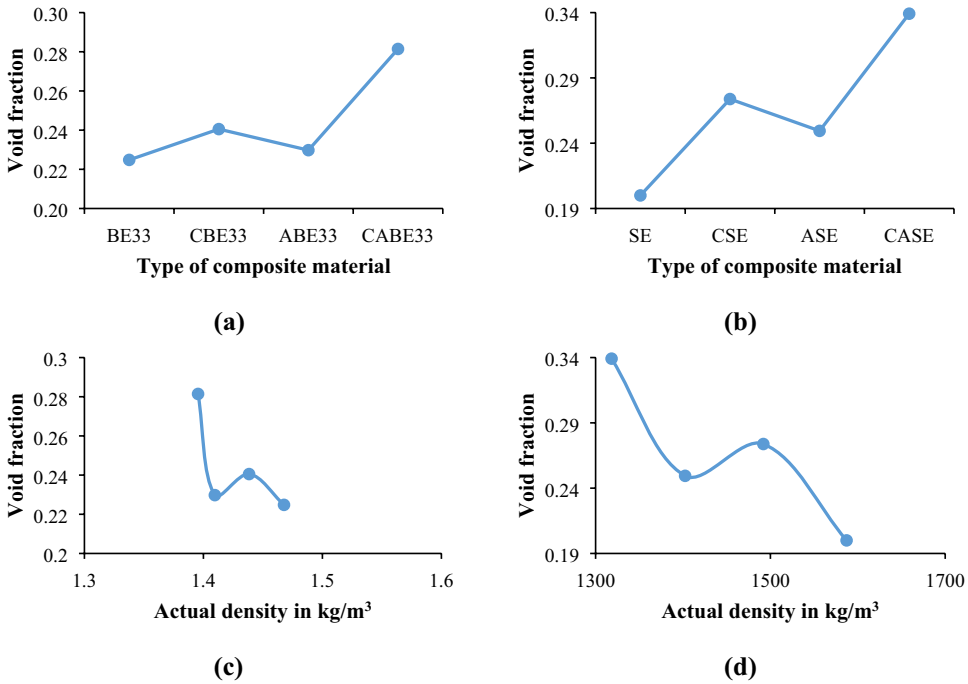

Fig. 2 Coir fiber/TiC nanoparticles reinforced epoxy composites **a** void fraction of bioepoxy composites **b** void fraction of synthetic epoxy composites, linear correlation between the actual density and void fraction **c** bioepoxy and **d** synthetic epoxy

CABE33, and ASE. The asymmetric and symmetric stretching vibration appeared in the range of 2850–3000 cm^{-1} assigned to CH_2 and CH_3 bending, which is absent in BE33, ABE33, and ASE composites [54]. From Tables 2 and 3, it is also observed that the bands 1385–1370 cm^{-1} and 1612–1609 cm^{-1} are assigned to the C–H bending and C=C stretching of the groups in carbohydrates [53]. Similarly, the C–H bending is absent in ABE33, SE, and ASE samples. The potential bands 1510–1509 cm^{-1} and 1460–1459 cm^{-1} correspond to the NO_2 asymmetric stretching and N–H stretching, respectively, which signifies the aromatic vibration of lignin content. Also, a small band 964–737 cm^{-1} was assigned to C–H out of plane bending deformation, which is also depicted in Tables 2 and 3 for bio and synthetic epoxy, respectively [53, 55]. Due to the presence of different functional groups, the complex behavior of the polymers, and the content of TiC nanoparticles, it is challenging to differentiate between the FTIR spectrum of with and without TiC nanoparticles in bio and synthetic epoxy composites. Ceramic particles commonly show absorptions between 940 and 500 cm^{-1}, while TiC exhibits the characteristics of Ti–C absorption in the wavenumber between 500 and 600 cm^{-1} [56]. The main difference reported in the FTIR spectrum of both pure epoxy and TiC reinforced epoxy composites is the occurrence of a weak Ti–C absorption under the wavenumber 600–450 cm^{-1} for ABE33, CABE33, ASE, and CASE samples which affirms the presence of TiC nanoparticles within the polymer matrix. The absence of epoxide oxirane ring (C–O–C) in the wavenumber of 900–940 cm^{-1} and amide II band for N–H bending at 1552–1541 cm^{-1} signifies the formation of linkages between the matrix and reinforced fillers and complete curing of the polymeric matrix respectively, whereas the N–H bending is absent in BE33, ABE33, SE, and ASE composites [57, 58].

Table 4 Effect of coir micro-fiber/TiC nanoparticles on density and void fraction of epoxy composites

	Actual density	Theoretical density	Void fraction (V_f)
BE33	1137.77	1467.73	0.22
CBE33	1092.41	1438.37	0.24
ABE33	1085.71	1409.61	0.23
CABE33	1002.76	1395.51	0.28
SE	1269.73	1587.17	0.20
CSE	1083.44	1491.94	0.27
ASE	1052.61	1402.43	0.25
CASE	871.16	1318.28	0.34

Effect on Physical Properties

Density

The information of void content and density in a specific epoxy polymer composite is necessary to measure nature. The actual density, void fraction, and theoretical density of these composites were determined as per the standards, and the outcomes are shown in Table 4. The theoretical density of epoxy composites, determined from Eq. (2), reduced with the addition of coir fiber or TiC nanoparticles, and a similar trend is also examined in the actual density of epoxy

composites. The actual densities calculated from Eq. (1) are comparably lower than the theoretical quantities and decreased remarkably with the reinforcement of fillers. Table 4 displays that the sample without any filler content has an actual density of 1137.77 kg/m^3 and 1269.73 kg/m^3 for BE33 and SE polymers respectively, which is considered as the reference point to interpret the decrement trend in densities with the reinforcement of coir fiber or TiC nanoparticles or both. The decrement in the actual density of 1092.41, 1085.41, 1002.76, 1083.44, 1052.61, and 871.16 kg/m^3 has been recognized for the CBE33, ABE33, CABE33, CSE, ASE, and CASE composites respectively. In both the composite samples CABE33, and CASE showed higher void fraction as 0.28 and 0.34, which is not acceptable to fabricate a composite, though it is utilized in the investigation to determine the effect of the addition of both coir fiber and TiC nanoparticles on epoxy polymer composites. There is a significant deviation between the theoretical and actual density of the epoxy composites, which is associated with the void content, as shown in Table 4. The production of voids is generally taken place because of the entrapment of air bubbles within the polymer matrix during the process of composites manufacturing [59]. The fraction of void was calculated from Eq. (3) and sketched as a function of the type of composites in Fig. 2a and b for bio epoxy Sr33 and synthetic epoxy, respectively. The formulation can be indicated from the polynomial equation with a suitable adjusted R squared quantity of 0.9358 and 0.951 representing the acceptability of the Eqs. (5) and (6) with 93.6% and 95.1% efficiency for bio and synthetic epoxy composites respectively.

$$V_{fBE} = 0.2493 + 0.2206 \times (FC)^{0.1224} \tag{5}$$

$$V_{fSE} = 0.1842 + 0.2022 \times (FC)^{0.3209} \tag{6}$$

where V_{f33} is a fraction of void for bio epoxy Sr 33, and FC is filler content in wt% (either coir fiber or TiC nanoparticles or both). The positive power exponent of filler content signifies that the fraction of voids increases with the addition of coir fiber or TiC nanoparticles. The polynomial formulation can be examined between void fraction and actual density, as presented in Fig. 2c and d for bio epoxy Sr33 and synthetic epoxy composites, respectively, where V_f proportionally reduced with incrementing the actual density because of negative slope of the curve. The formulation can be showed and derived in Eqs. (7) and (8) for bio and synthetic epoxy composites, respectively.

$$V_f = 0.022 + 0.7693 \times {\rho_{act}}^{3.24} \tag{7}$$

$$V_f = 2.012 + 0.6351 \times {\rho_{act}}^{2.41} \tag{8}$$

The polynomial Eqs. (7) and (8) has an adjusted regression quantity of 0.999, which exhibits the polynomial formulation with approximately 99.9% fit. Hence, it can be observed that the addition of coir fiber or TiC nanoparticles should significantly increment the void content of the epoxy composites. The similar results has been observed from Pattanaik et al. for the fly ash filled epoxy composites.

Contact angle

The chemical behavior of the epoxy composite surface is established by the wetting principle, which is broadly investigated for practical utilization: for example, as self-cleaning or protective materials [60, 61]. Wetting capacity assigns to the water droplet degree dispersed on the composite surface, and it simply observed from the water contact angle. Figure 3a–h displays the contact angle measurements for BE33, CBE33, ABE33, CABE33, SE, CSE, ASE, and CASE composites. The chemistry and phenomenon of surfaces considering the determined contact angle are shown in Fig. 3i. The wetting capacity of the surface is higher if the contact angle is lower, for instance, the surface energy at the epoxy polymer composite interface, where the size of the water droplet is higher, which can be denoted as hydrophilic. In the same context, if the contact angle is more than 90° which exhibit the hydrophobic behavior of the composites. Figure 4 shows the left and right side of the contact angle of bio and synthetic epoxy composites reinforced with coir fiber or TiC nanoparticles or both fillers. The pure bio epoxy Sr 33 and synthetic epoxy polymer show the hydrophilic behavior with 73.66° and 81.4° of contact angle, respectively. The addition of coir fibers or TiC nanoparticles within the bio epoxy Sr 33 reduces the contact angle up to 67.38°, which signifies the increment in surface energy and hydrophilicity. Whereas the reinforcement of both fillers in synthetic epoxy slightly increments the contact angle till 82.5°. These outcomes also signify that a decrement in hydrophilicity in synthetic epoxy-based composites is observed when compared with bio epoxy. It is considered that the addition of TiC nanoparticles in the synthetic epoxy composites produced a compressed composite sample, which offers reduced sticky load when with the cohesive interior loads in the water droplets by incrementing the contact angle [62]. The uniform dispersion of both coir fiber and TiC nanoparticles in the laminates shows the reduction in hydrophilicity of the synthetic epoxy composites when compared with bio epoxy samples. Similar outcomes has been observed by Kocijan et al. [61] and Ali et al. [62] for TiO2 reinforced high-performance epoxy composite coatings.

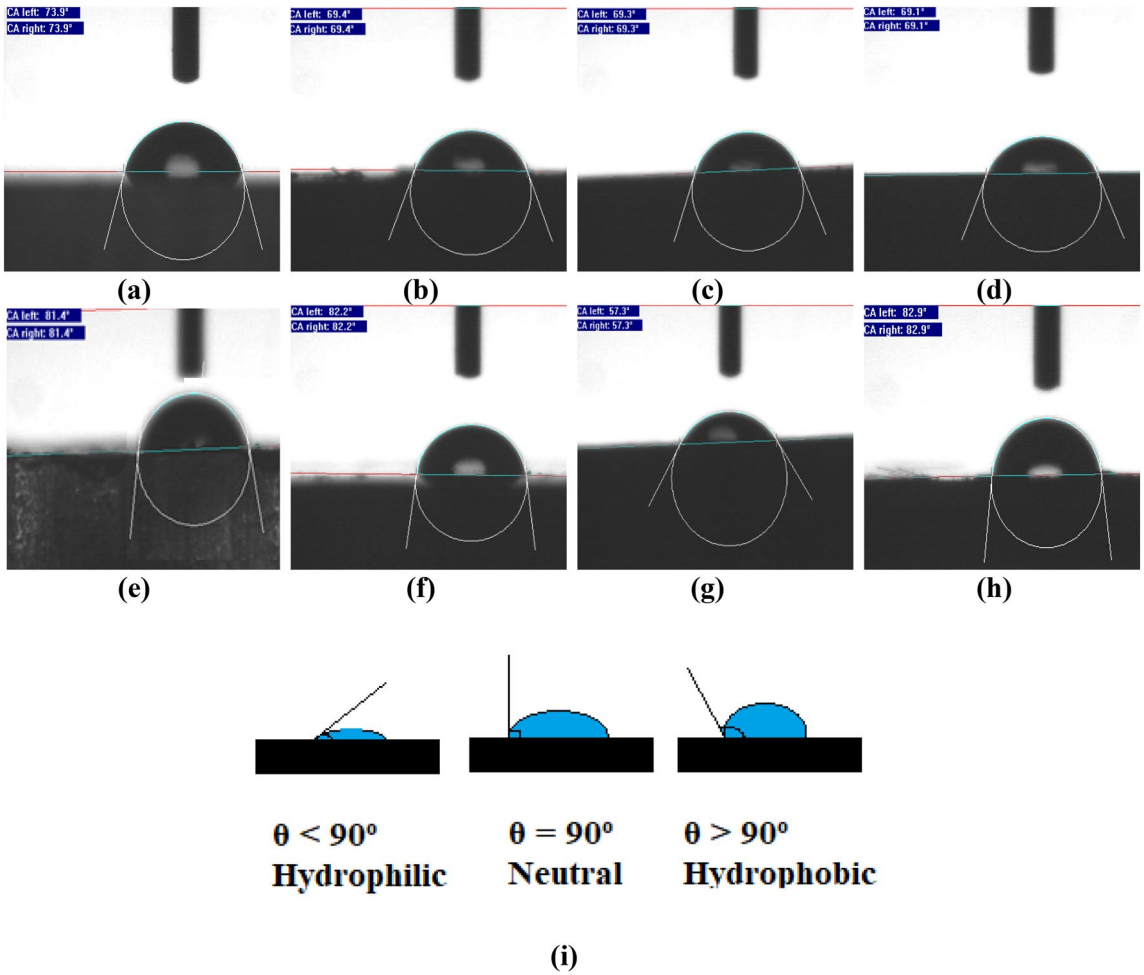

Fig. 3 Contact angle measurement displaying water droplets on the surface of epoxy composites **a** BE33, **b** CBE33, **c** ABE33, **d** CABE33, **e** SE, **f** CSE, **g** ASE, **h** CASE, and **i** the chemistry and phenomenon of surfaces considering the determined contact angle

Porosity

The porosity level was measured for every epoxy composite samples, based on the formation of void during the mixing of fillers within the matrix, as per the recent literature Hamid et al. [63], the examination of porosity from microscopic analysis which offers the best characteristics around the thickness of the composites. Hence, the porosity characterization was conducted by polarized optical microscope from the thickness of samples, under the 200 x magnification using ImageJ software. After the reinforcement of coir fibers, the porosity of both the epoxy matrix composites increased (Fig. 5), due to the higher hydrophilicity as observed in contact angle measurements. While the TiC nanoparticles reinforced composites showed a porosity of 5.48% and 5.28% for ABE33 and ASE composites respectively since the TiC nanoparticles preform exhibited a higher impregnation degree [64, 65]. As observed, the coir fiber/TiC nanoparticles reinforced hybrid composite offered transitional porosity outcome with a quantity of 4.17% for CABE33 and 2.05% for CASE composites. The TiC nanoparticles were responsible for the reduction of porosity level, which is assigned with the uniform dispersion of fillers

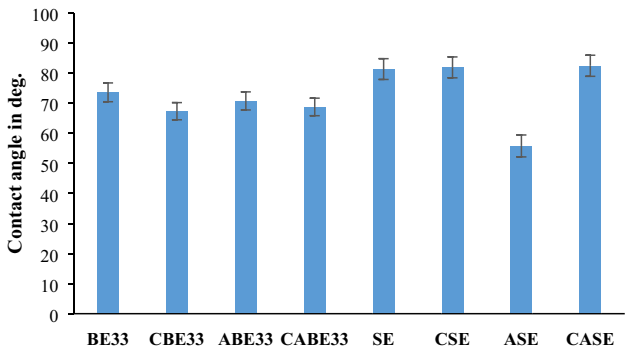

Fig. 4 Contact angle measurement of coir fiber/TiC nanoparticles reinforced epoxy composites

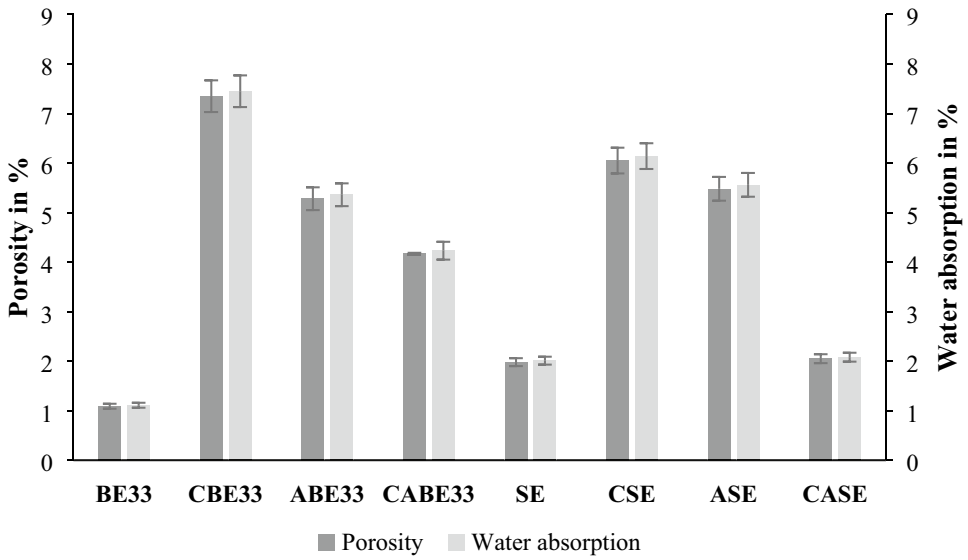

Fig. 5 Porosity and water absorption characteristics of coir fiber/TiC reinforced epoxy composites. **a** Contact angle, and **b** Porosity and water absorption

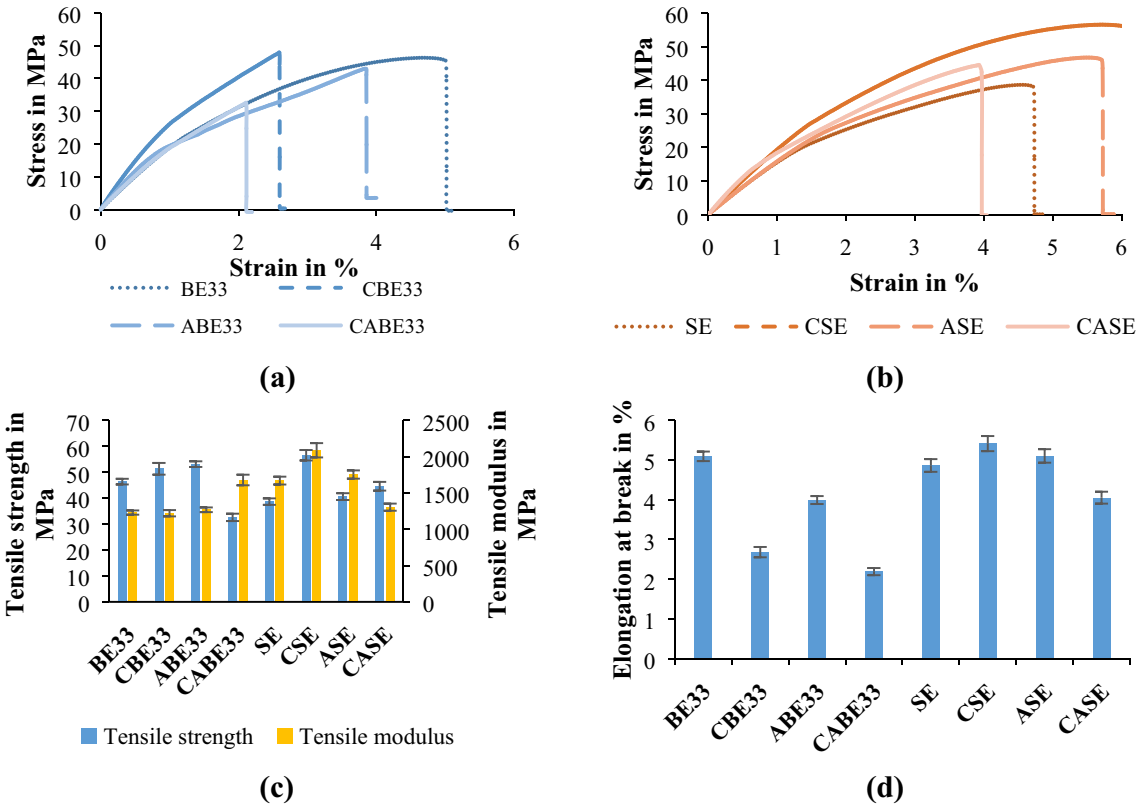

Fig. 6 Tensile properties of coir fiber/TiC reinforced epoxy composites. **a** Stress–strain curve of Bio-epoxy 33 composites, **b** Stress–strain curve of synthetic epoxy composites, **c** Tensile strength and modulus, **d** elongation at break

within the matrix, especially for the CASE composite, which is similar to the Monticelli et al. and Ornaghi et al. for glass and carbon epoxy laminates [66, 67].

However, in the optimized condition, the porosity of SAT epoxy hybrid nanocomposites have lower porosity content (Fig. 6b)than the other two types, due to the removal of hemicellulose and lignin content from chemical treatment. The improper impregnation of fibers and agglomeration of Al–SiC nanoparticles were observed in SRS and SST epoxy nanocomposites. From the

confirmation experiment, both SST and SAT epoxy hybrid nanocomposites also have lower water absorption capacity (Fig. 6b) as compared with SRS, due to lower concentration of hemicellulose, lignin, and stronger interfacial bonding within the SNCF/Al–SiC nanoparticles/epoxy matrix as observed from the FTIR and XRD analysis. However, in the optimized condition, the porosity of SAT epoxy hybrid nanocomposites have lower porosity content (Fig. 6b than the other two types, due to the removal of hemicellulose and lignin content from chemical treatment. The improper impregnation of fibers and agglomeration of Al–SiC nanoparticles were observed in SRS and SST epoxy nanocomposites. From the confirmation experiment, both SST and SAT epoxy hybrid nanocomposites also have lower water absorption capacity (Fig. 6b) as compared with SRS, due to lower concentration of hemicellulose, lignin, and stronger interfacial bonding within the SNCF/Al–SiC nanoparticles/epoxy matrix as observed from the FTIR and XRD analysis.

Water Absorption

Water absorption characteristics of the bio-epoxy and synthetic epoxy composites reinforced with coir fiber or TiC nanoparticles were measured for every composition. In Fig. 5, the water absorption quantity was observed to improve with the addition of coir microfibers in the polymer laminates. In this context, the polymer laminates CABE33 and CASE showed lower water absorption capacity. The sample CBE33 and CSE composites tend to ingest more moisture than other epoxy composite samples, which signified the increment in moisture absorption because of poor adhesion between the matrix and fiber. However, the ABE33 and ASE composites had better adhesion, which had lower moisture content to consume when compared with CBE33 and CSE composites and similar results was observed by Ahad et al. [68].

Effect on Mechanical Properties

Tensile Properties

The stress–strain graphs of neat bio-epoxy, synthetic epoxy, and their respective coir fiber or TiC nanoparticles reinforced composites are shown in Fig. 7a and b. Both the epoxy polymers, the stress–strain graphs under room temperature exhibited non-linear sections. In general, the tensile strength, and modulus of CBE33, ABE33, CSE, and ASE were more significant than that of the respective pure epoxy polymer (Fig. 7c), signifying that the addition of coir fiber or TiC nanoparticles can enhance the tensile characteristics of the epoxy polymer. The CBE33, ABE33, CSE, and ASE improved the tensile strength by 10.66%, 12.7%, 46.24%, and 4.99%, respectively, compared with their respective pure bio and synthetic epoxy polymers and also found that the failure strain of the respective composites was enhanced [69]. Figure 7d exhibits the elongation at break with the type of epoxy polymer composites. The

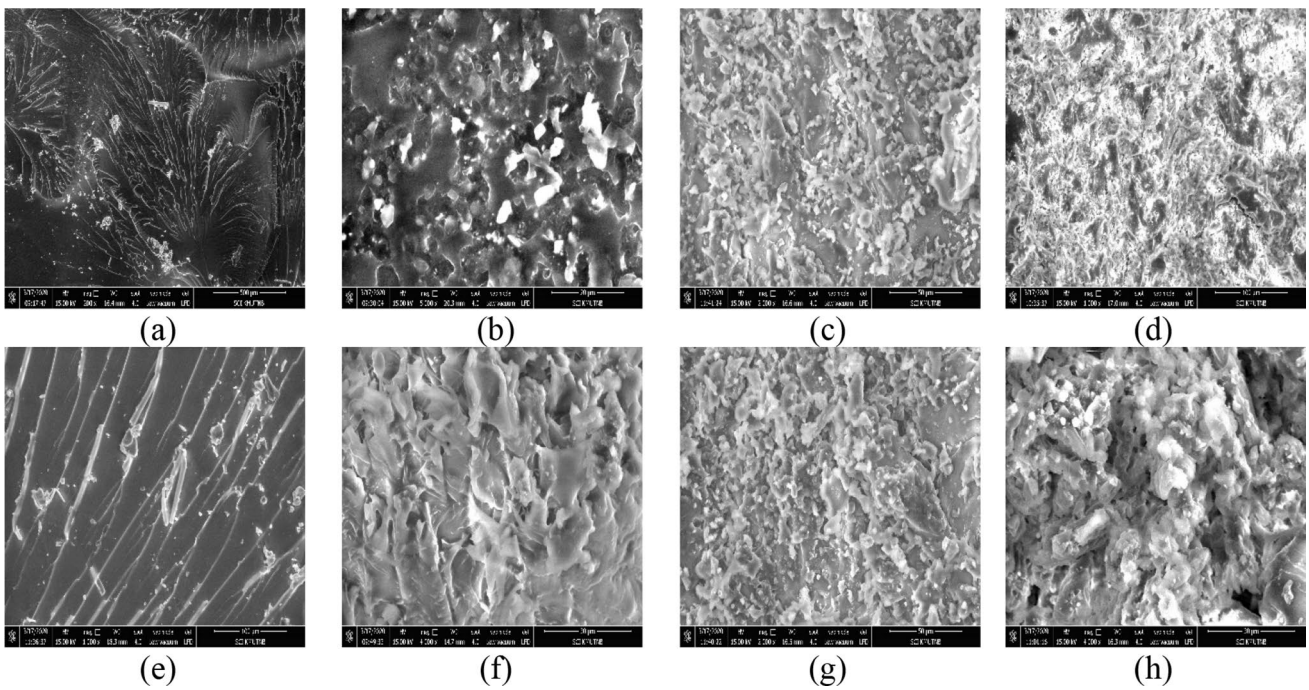

Fig. 7 Tensile fracture of coir fiber/TiC reinforced epoxy composites **a** BE33, **b** CBE33, **c** ABE33, **d** CABE33, **e** SE, **f** CSE, **g** ASE, **h** CASE

elongation at break attained a higher value of 5.41% for CSE composite, which was 11.32% higher when compared with pure synthetic epoxy (4.86%). The reinforcing principle of CSE epoxy primarily associated the dissipation of energy mechanisms. The formation of shear bond and plastic void growth affected from coir fiber micro-particles or TiC nanoparticle and debonding was the primary method for the dissipation of energy. Johnsen et al. Liang et al. and Zhang et al. for nano-silica based epoxy nanocomposites also affirmed the similar result of principle of energy dissipation [70–72]. However, the distinct from other investigations, the TiC nanoparticles in the present work were bonded covalently to polymeric epoxy networks, which improved the stronger interfacial bonding. Therefore, the tensile strength of both epoxy polymer was efficiently enhanced by incorporating suitable reinforcement material, either coir or TiC nanoparticles. Furthermore, the tensile properties of CABE33 and CASE composites were observed to be decreased with the addition of both coir fiber and TiC nanoparticles, which is primarily assigned to the accumulation, reduced the reinforcing effect, and also weakened the crosslinking density of polymeric epoxy networks [73]. Yao et al. [74] and Dittanet and Pearson [75] also observed the similar outcomes for free grapheme/carbon nanotube/Fe3O4 epoxy and silica filled epoxy composites respectively.

Tensile Fracture

The fracture microstructure of BE33, CBE33, ABE33, CABE33, SE, CSE, ASE, and CASE epoxy composites are shown in Fig. 8a–h respectively. The common consent is that the fracture surface of both epoxy polymers has cleavage structures, which is aligned with the generation of cracks, shown in Fig. 8a and e [76]. The production of shear bands was also examined on the fracture surface, signifying that higher dissipation energy appeared during the propagation of crack [77]. After the reinforcement of coir fibers in bio and synthetic epoxy, it was examined that the fibers were uniformly dispersed and bonded within the epoxy polymer matrix in Fig. 8b and f, which improved the tensile properties of both composites. While comparing the Fig. 8c and g, the fracture surface of bio epoxy and synthetic epoxy consists of TiC nanoparticles were relatively rough surface, and the production of the shear band also not noticeable. The primary reason was the accumulation of particle size to form larger sizes, which weakened the reinforcing impact of TiC

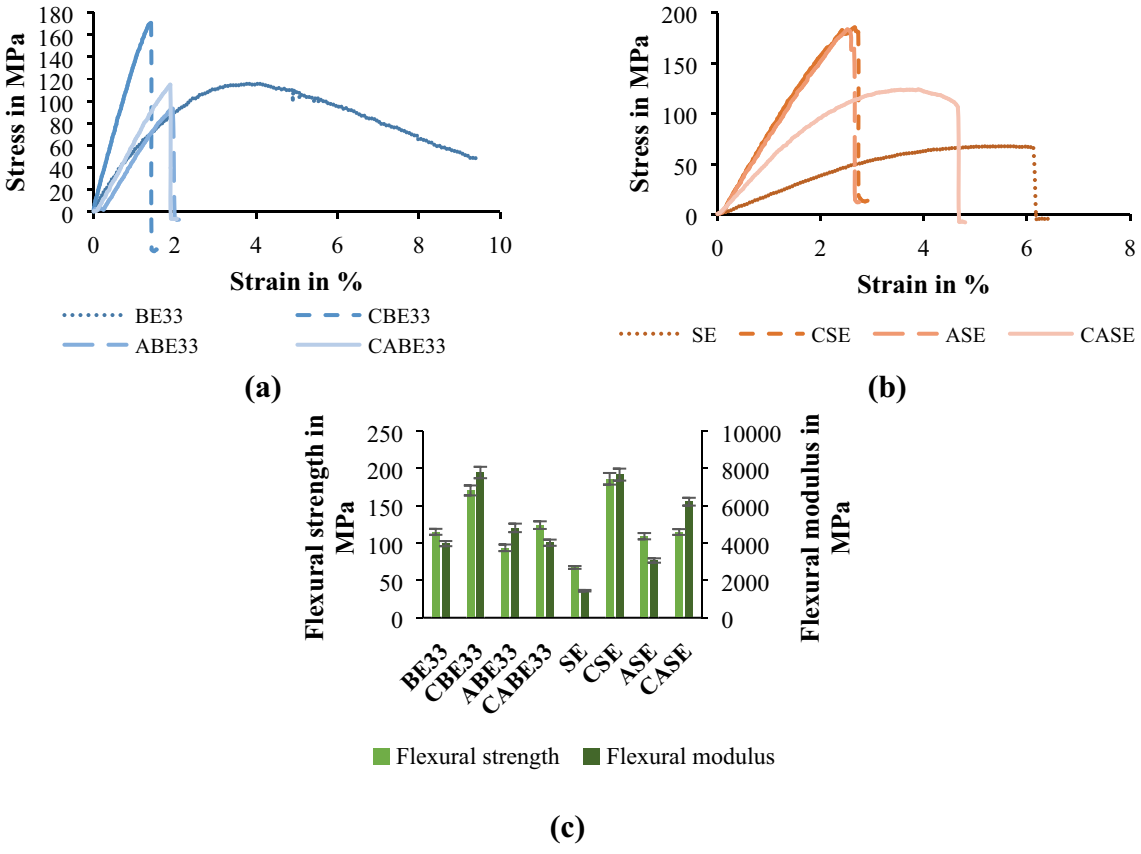

Fig. 8 Flexural properties of coir fiber/TiC reinforced epoxy composites. **a** Stress–strain curve of Bio-epoxy 33 composites, **b** Stress–strain curve of synthetic epoxy composites, **c** Flexural strength and modulus

nanoparticles within the polymer matrix, which reduced the tensile properties of the composites [69].

Nevertheless, the addition of both particles such as coir fiber and TiC nanoparticles (Fig. 8d and h) leads to the accumulation of particles, which shows the debonding at the interface between the fillers and matrix. These are the proof for wear and weak interfacial bonding, which generally affect the bonding strength at the interface, and load transfer at the interface also reduced, which decreases the tensile properties of the epoxy composites. This rough surface in these conditions does not permit the appropriate bonding within the matrix and reinforced fillers when fabricating the composites. Similar investigations have been observed by Oladele et al. [78] Li et al. [73] and Kothmann et al. [77] for modified palm kernel shell fiber/particulate cassava peel hybrid epoxy, nano-SiO_2/epoxy-functionalized polysiloxane, and silica nano-particles respectively.

Flexural Properties

Figure 9a, b shows the stress–strain graphs of bio and synthetic epoxy composite reinforced with coir fiber or TiC nanoparticles or both. The stress here incremented linearly with increased strain till the specimen fails. The incorporation of TiC nanoparticles also decreased the flexural properties of the epoxy composites, which also followed the trend of tensile strength and modulus. Figure 9c displays the flexural strength and modulus, which depending on the type of reinforcement either coir fiber or TiC nanoparticles or both with the bio and synthetic epoxy matrix. The addition of TiC nanoparticles in the coir/bio improved the flexural strength and modulus from 115.05 to 124 MPa and 3970.5 to 4813.2 MPa respectively, whereas coir/synthetic epoxy enhanced the flexural strength and modulus up to 114.82 MPa and 6215.9 MPa respectively when compared with their respective neat polymer. The highest flexural strength of 170.48 MPa and 186.05 MPa is attained for CBE33, and CSE composites, which is 27.26%, and 38.28% is higher than the CABE33 and CASE composites respectively. TiC nanoparticles enhance the mechanical bonding within the coir fiber and epoxy polymer in the interphase section, hence improving the flexural strength when compared with neat polymers [35, 39]. By reinforcing TiC nanoparticles in ABE33, the flexural strength reduced to 93.65 MPa, and the accumulation of nanoparticles in the polymer matrix is the major reason for the decrement in flexural properties [79] whereas the ASE increased up to 109.21 MPa, due to the uniform dispersion of nanoparticles and stronger interfacial bonding within the polymeric matrix [76]. Similar results has been observed by the Mohit and Selvan [76] and Bulut et al. [79] for the Al–SiC/epoxy and basalt/grapheme/epoxy nanocomposites respectively.

Impact Strength and Shore Hardness

Figure 6 presents the impact strength of the bio and synthetic epoxy composites reinforced with coir fiber or TiC nanoparticles. It was examined that the CBE33, CABE33, CSE, and CASE have higher impact strength when compared with their respective neat polymers, which may improve the pull out load, due to the uniform dispersion of fibers within the matrix [80]. The impact strength mainly depends on fiber resistance during fracture, and dispersion has more capability to absorb a high amount of energy during the testing process [81]. From the results, it is observed that the ABE33 and ASE have a lower impact strength of 1.29 and 1.26 kJ/m^2, respectively, due to the agglomeration of nanoparticles, and weaker bonding

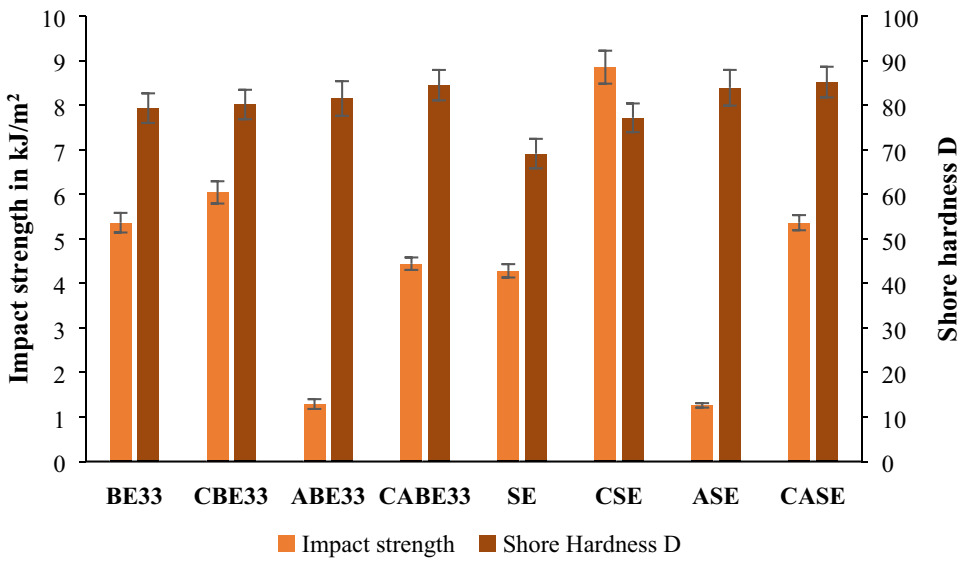

Fig. 9 Impact strength and shore hardness of coir fiber/TiC reinforced epoxy composites

within their respective polymer matrices. Similar results of improvement in impact strength of the epoxy composites is observed in Mohit and Selvan [80], for sugarcane nanocellulose fiber/aluminum silicon carbide reinforced epoxy hybrid nanocomposites.

The calculated shore hardness D quantities of bio and synthetic epoxy composites are shown in Fig. 6. The hardness of both epoxy composites is improved with the addition of coir fiber or TiC nanoparticles or both, due to the fillers and matrix are cross-linked covalently, hence producing a robust interfacial bonding within the matrix and filler. As we observed that the TiC nanoparticles have excellent mechanical characteristics, hence reinforcing TiC nanoparticles can improve the mechanical characteristics of the polymer composites, which is similar to the Zheng et al. [82] and Papageorgiou et al. [83] for graphene based epoxy composites.

Thermal Characteristics

Figures 10a, b and 11a, b show the TG and DTG curves, respectively, of bio-epoxy and synthetic epoxy composites. In this condition, this mechanism did not obstruct in determining a first stage loss (5%) of weight up to 190 °C, assigned to the evaporation of residual moisture content from the composites. In the second stage, the higher

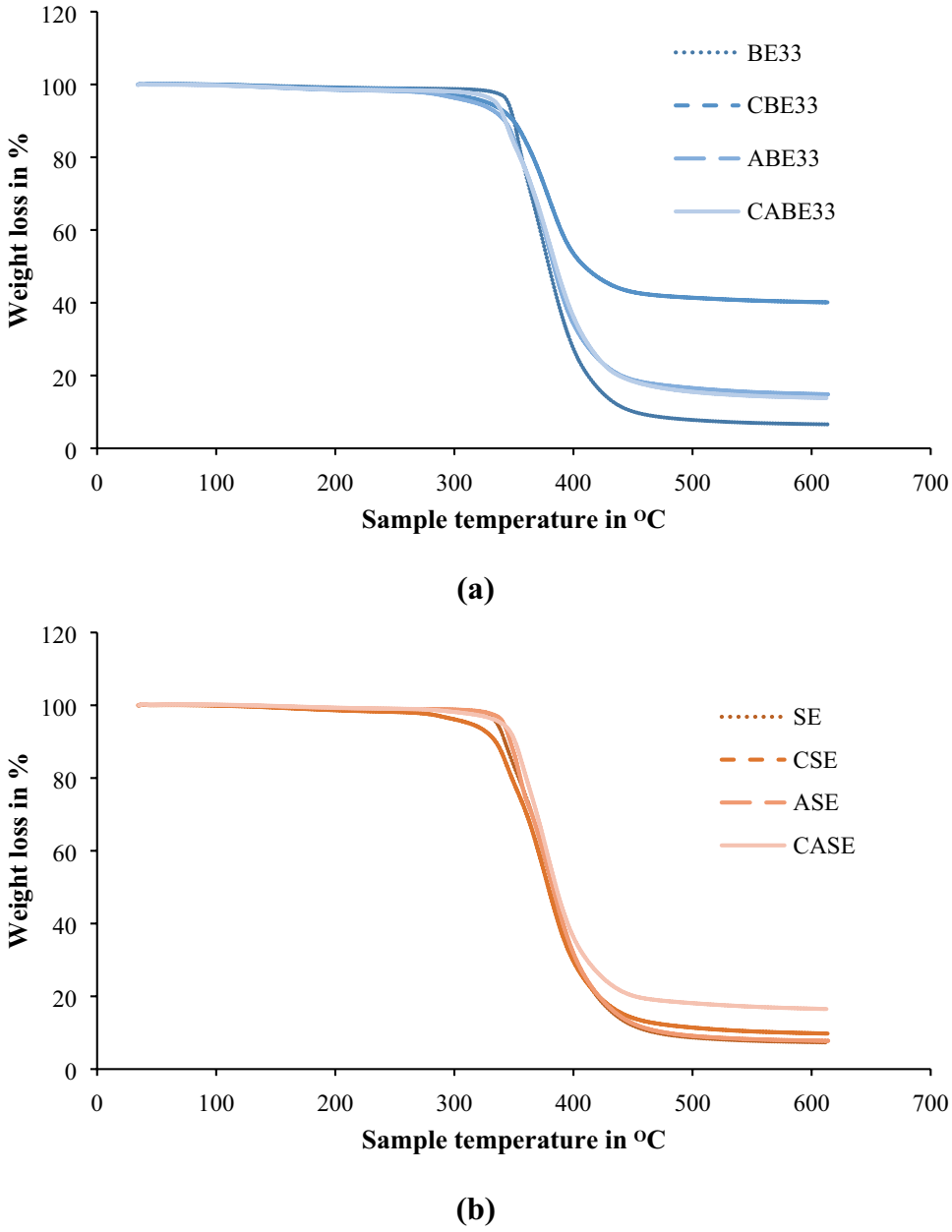

Fig. 10 TG curves of coir fiber/TiC reinforced epoxy composites. **a** Bio-Epoxy 33 and **b** Synthetic epoxy composites

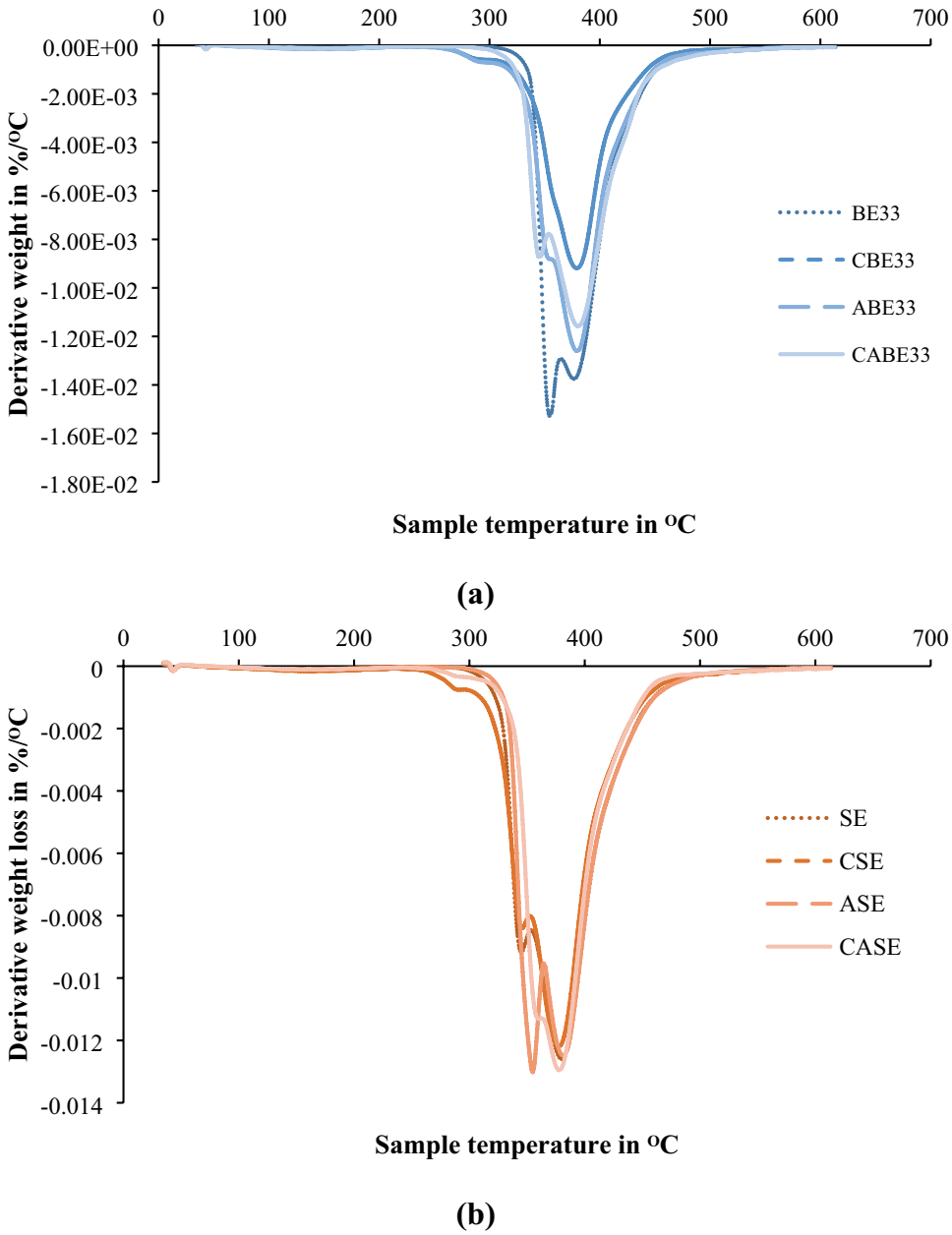

Fig. 11 DTG curves of coir fiber/TiC reinforced epoxy composites. **a** Bio-Epoxy 33 and **b** Synthetic epoxy composites

Table 5 Thermal characteristics of coir fiber/TiC reinforced hybrid epoxy composites

	Transition mass loss in %	Onset temperature in °C	Endset temperature in °C	Carbon residue in %
BE33	– 89.26	335.63	384.78	6.57
CBE33	– 72.13	338.02	396.9	10.14
ABE33	– 75.8	338.24	397.71	13.81
CABE33	– 79.65	334.51	402.71	14.82
SE	– 88.43	334.04	403.67	7.32
CSE	– 83.66	330.48	398.19	9.77
ASE	– 85.15	331.1	394.63	11.29
CASE	– 77	339.28	398.11	16.52

weight loss has occurred between 200 and 500 °C is attributed to the degradation of constituents of materials, which is known sequence, due to thermoset polymers have lower resistance from higher temperature beyond 250 °C [53]. Table 5 shows the related thermogravimetric factors for the graphs in Figs. 10 and 11. From the TG graphs, and Table 5, the onset temperature for extreme deterioration, after the evaporation of moisture content is around 330 °C and not much influenced by the coir fiber or TiC nanoparticles or both the content in the polymer matrices. Also, this would correspond to the maximum thermal resistance of epoxy polymers, and it is suggested that the maximum temperature working for these epoxy composites up to 260 °C when

compared with Buriti fibers observed by Demosthenesa et al. [53]. As observed in Table 5, the maximum degradation appeared at 384.78 °C, which was affected by the dehydration process when compared with Levchik et al. [84] and Grassie et al. [85]. The production of carbonaceous char during the thermal deterioration under higher temperatures could be oxidized in atmospheric air and limited char of 6.57 wt% and 7.32 wt% for neat bio epoxy Sr33 and synthetic epoxy under 600 °C. With specimen CBE33 and CSE, which was fabricated from the reinforcement of 10 wt% of coir fiber, the deterioration ensued at a lower end set temperature of 396.9 °C and 398.19 °C, which is comparably higher than the BE33, and SE composites respectively. The carboxylic acid created from the coir fiber could comprise the hydroxyl group of epoxy polymer in air, which would further produce a compact layer under a higher range of temperature [80, 86]. Hence, the residue of char and thermal stability improved until 10.14% for CBE33 and 9.77% for CSE when compared with their respective neat polymers. For specimen ABE33 and ASE composites, which consists of 10 wt% of TiC nanoparticles, the corresponding end set temperatures are 397.71 °C and 394.63 °C, because the TiC nanofillers have the melting point of 3065 ºC [48]. For the bio-epoxy sample, the degradation temperature improved, whereas, in synthetic epoxy, reduction is observed. Specimen CABE33 and CASE were fabricated with 5 wt% of coir fiber and 5 wt% of TiC nanoparticles separately, where the end set temperature of the composites increased to 402.71 °C and 398.11 °C respectively. As in the epoxy polymer, the CABE33 and CASE also contain hydroxyl groups observed in FTIR spectra, and it could also comprise the aromatic functional groups of the epoxy polymer during the degradation process. It is recommended that the CABE33 composite could agree with the epoxy hybrid composites to produce a highly efficient protective layer, which is similar to Levchik et al. [84] Grassie et al. [85] and Zheng et al. [82] carbon fiber epoxy, degradation of epoxy, and grapheme based epoxy composites investigations.

Table 6 Resistance of Bio-epoxy 33 and synthetic epoxy composites against the interaction of chemicals after soaking in 10 wt% of NaCl, 10 wt% of NaOH and 30 wt% of H_2SO_4 solution under room temperature with 65 ± 2% of relative humidity

	10 wt% of NaCl	10 wt% of NaOH	30 wt% of H_2SO_4
BE33	−	−	−
CBE33	+	+	+
ABE33	+	+	+
CABE33	+	+	+
SE	−	−	−
CSE	+	+	+
ASE	+	+	+
CASE	+	+	+

Chemical Resistance Characteristics

The chemical resistance investigations were conducted by soaking the fabricated epoxy samples in different types of chemicals such as 10 wt% of NaCl, 10 wt% of NaOH, and 30 wt% of H_2SO_4 solutions. After the soaking process, the composite samples were observed for cracking, blistering, or any other attack from the solvent. The outcomes of the chemical resistance of the fabricated epoxy composites are shown in Table 6, which establishes that all the fabricated samples have excellent resistance from acids up to 15 days. Furthermore, the blistering and cracking are observed in BE33, CBE33, SE, and CSE samples soaked in the alkali solutions. The unsaturated networks and residual hydroxyl groups could tend to bad alkali resistance of the polymer composites [87]. It is suggested that the alkali resistance can be enhanced by reducing the hydroxyl content and reducing the cross-linking degree with the addition of both coir fiber and TiC nanoparticles. Similar outcomes has been observed by the Mohit and Selvan [80], and Bai et al. [87] for sugarcane nanocellulose fiber/aluminum silicon carbide epoxy and polyacrylate/SiO_2 urushiol formaldehyde polymer respectively.

Conclusions

In the present investigation, the effect of coir fiber and TiC nanoparticles on the physical, mechanical, and thermal characteristics of bio and synthetic epoxy composites has been explored. The addition of coir fiber and TiC nanoparticles significantly enhanced the epoxy composite characteristics. The outcomes of the investigation on the characteristics of TiC nanoparticles reinforced coir fiberf/epoxy composites have shown the following conclusions:

- CABE33, and CASE showed higher void fraction as 0.28 and 0.34, which is not acceptable to fabricate a composite, and the production of voids are taken place because of the entrapment of air bubbles within the polymer matrix during the manufacturing process.
- The addition of coir fibers or TiC nanoparticles within the bio epoxy Sr 33 reduces the contact angle up to 67.38°, which signifies the increment in surface energy and hydrophilicity. It is also observed that the addition of coir fiber and TiC nanoparticles in the synthetic epoxy composites produced a compressed composite sample, which offers reduced sticky load when with the cohesive

interior loads in the water droplets by incrementing the contact angle.

- The addition of TiC nanoparticles and coir fiber was responsible for lower porosity levels for CABE33 and CASE as 4.17% and 2.05%, respectively, when compared with CBE33 and CSE composites.
- The CBE33, ABE33, CSE, and ASE improved the tensile strength by 10.66%, 12.7%, 46.24%, and 4.99%, respectively, compared with their respective pure bio and synthetic epoxy polymers.
- The highest flexural strength of 170.48 MPa and 186.05 MPa is attained for CBE33, and CSE composites, which is 27.26%, and 38.28% is higher than the CABE33 and CASE composites respectively.
- The tensile and flexural properties of CABE33 and CASE composites was observed to be decreased with the addition of both coir fiber and TiC nanoparticles, which is primarily assigned to the accumulation as observed in SEM analysis, reduced the reinforcing effect, and also weakened the crosslinking density of polymeric epoxy networks.
- It is found that the ABE33 and ASE have a lower impact strength of 1.29 and 1.26 kJ/m^2, respectively, due to the agglomeration of nanoparticles, and weaker bonding within their respective polymer matrices.
- The hardness of both the epoxy composites is improved up to 85.16 with the addition of coir fiber or TiC nanoparticles or both, due to the fillers and the matrix are cross-linked covalently, hence producing a robust interfacial bonding within the matrix and filler.
- The residue of char and thermal stability improved until 10.14% for CBE33 and 9.77% for CSE when compared with their respective neat polymers.
- The blistering and cracking are observed in BE33, CBE33, SE, and CSE samples soaked in the alkali solutions due to the unsaturated networks and residual hydroxyl groups, which tend to bad alkali resistance of the polymer composites.

Further research investigations needs to be explore on effect of synthetic fiber, number of layers, nature of bonding with other type of polymer matrix. Besides, investigation also need to be performed for electrical, and dielectric properties to develop the material for electromagnetic shielding applications.

Acknowledgements This project was funded by the Deanship of Scientific Research (DSR) at King Abdulaziz University, Jeddah, under grant no. KEP-50-130-38. The authors, therefore, acknowledge with thanks DSR for technical and financial support. The research was funded by King Mongkut's University of Technology North Bangkok with Contract no. KMUTNB-Post-64-06.

References

1. Ramesh M, Palanikumar K, Reddy KH (2017) Renew Sustain Energy Rev 79:558–584
2. Ku H, Wang H, Pattarachaiyakoop N, Trada M (2011) Compos Part B Eng 42:856–873
3. Thakur VK, Thakur MK (2014) Carbohydr Polym 109:102–117
4. Abdul Khalil HPS, Bhat AH, Ireana Yusra AF (2012) Carbohydr Polym 87:963–979
5. Ezekiel N, Ndazi B, Nyahumwa C, Karlsson S (2011) Ind Crops Prod 33:638–643
6. Akil HM, Omar MF, Mazuki AAM, Safiee S, Ishak ZAM, Bakar AA (2011) Mater Des 32:4107–4121
7. Lecompte T (2012) Constr Build Mater 78:224–233
8. Saw SK, Sarkhel G, Choudhury A (2011) Appl Surf Sci 257:3763–3769
9. Rahman MM, Khan MA (2007) Compos Sci Technol 67:2369–2376
10. Silva GG et al (2000) J Appl Polym Sci 76:1197–1206
11. Zhang L, Hu Y (2014) Mater Des 55:19–26
12. Pickering KL, Efendy MGA, Le TM (2016) Compos Part A. Appl Sci Manuf 83:98–112
13. Mir SS, Nafsin N, Hasan M, Hasan N, Hassan A (2013) Mater Des 52:251–257
14. Kumar SMS, Duraibabu D, Subramanian K (2014) Mater Des 59:63–69
15. Fiore V, Di Bella G, Valenza A (2015) Compos Part B Eng 68:14–21
16. Abdul AHR, Roslan A, Jaafar M, Roslan MN, Ariffin S (2011) Adv Mater Res 277:36–42
17. Prajapati P, Sharma C, Rana RS (2018) Mater Today: Proc 5(9):19056–19062
18 Nagarjun J, Kanchana J, Kumar GR (2020) J Nat Fiber 5:1–10
19 Shahzad A, Nasir SU (2017). In: Jawaid M, Sapuan S, Alothman OY (eds) Green biocomposites. Springer, Cham
20. Anbukarasi K, Hussain SI, Roseline AA, Kalaiselvam S (2019) Mater Res Exp 6:125618
21. Sumesh KR, Kanthavel K (2020) Polym Bull 77:4609–4629
22. Geng R, Qiu F, Jiang QC (2018) Adv Eng Mater 20(9):1701089
23. Faridirad F, Ahmadi S, Barmar M (2017) Polym Eng Sci 57(5):475–494
24. Horszczaruk E (2019) Mater 12(2):326:1–326:34
25. De Cicco D, Asaee Z, Taheri F (2017) Nanomater 7(11):360
26. Lu X, Liu C, Hu G, Xuan X (2017) J Colloid Interface Sci 500:182–201
27. Rokni MR, Nutt SR, Widener CA, Champagne VK, Hrabe RH (2017) J Therm Spray Technol 26(6):1308–1355
28. Jiang CC, Cao YK, Xiao GY, Zhu RF, LU YP (2017) RSC Adv 7(13):7531–7539
29. Li Q, Liao G, Zhang S, Pang L, Tong H, Zhao W, Xu Z (2018) Appl Surf Sci 427:437–450
30. Feng Y, Ning N, Wei Z, Zhang L, Tian M, Zou H, Mi J (2014) Polym 55(14):3178–3185
31. Rianyoi R, Potong R, Ngamjarurojana A, Chaipanich A (2013) Ceram Int 39:S47–S51
32. Nam S, Cho HW, Lim S, Kim D, Kim H, Sung BJ (2013) ACS Nano 7(1):851–856
33. Pathak AK, Kumar V, Sharma S, Yokozeki T, Dhakate SR (2018) J Colloid Interface Sci 533:548–560
34. Alamri H, Low IM, Alothman Z (2012) Compos Part B Eng 43:2762–2771
35. Ary Subagia IDG, Tijing LD, Kim Y, Kim CS, Vista IVFP, Shon HK (2014) Compos Part B Eng 58:611–617

36. Bekyarova E, Thostenson ET, Yu A, Kim H, Gao J, Tang J, Hahn HT, Chou TW, Itkis ME, Haddon RC (2007) Langmuir 23:3970–3974
37. Seretis GV, Theodorakopoulos ID, Manolakos DE, Provatidiset CG (2018) Compos Part B Eng 147:33–41
38 Kamaraj M, Dodson EA, Datta S (2019) Adv Compos Mater 29:443
39. Pathak AK, Borah M, Gupta A, Yokozeki T, Dhakate SR (2016) Compos Sci Technol 135:28–38
40. Arbatti M, Shan X, Cheng Z (2007) Adv Mater 19(10):1369–1372
41 Kobayashi Y, Miyashiro H, Takeuchi T, Shigemura H, Balakrishnan N, Tabuchi M, Kageyama H, Iwahori T (2002) Solid state ionics. Elsevier, Amsterdam
42. Li K, Zeng DW, Yung KC, Chan HLW, Choy CL (2002) Mater Chem Phys 75(1–3):147–150
43. Jiang QC, Li XL, Wang HY (2003) Compos Scr Mater 48(6):713–717
44. Sahoo P, Koczak MJ (1991) J Mater Sci Eng A 131(1):69–76
45. Xiuqing Z, Haowei W, Lihua L, Xinying T, Naiheng M (2005) Mater Lett 59(17):2105–2109
46. Parashivamurthy KI (2001) J Mater Sci 36(18):4519–4530
47. Radja I, Djelad H, Morallon E, Benyoucef A (2015) Syn Metal 202:25–32
48. Durlu N (1999) J Eur Ceram Soc 19(13–14):2415–2419
49. Doˇgan ON, Hawk JA, Tylczak JH, Wilson RD, Govier RD (1999) Wear 225–229:758–769
50. Qing Y, Nan H, Luo F, Zhou W (2017) RSC Adv 7(44):27755–27761
51. El-Tantawy F (2002) Eur Polym J 38(3):567–577
52 Stuart B (2004) Infrared spectroscopy: fundamentals and applications. Wiley, New York
53. da Cruz Demosthenesa LC, Nascimento LFC, Monteiro SN, Costa UO, da Filho FCG, da Luz FS, Oliveira MS, Ramos FJHTV, Pereira AC, Braga FO (2020) J Mater Res Technol 9(1):115–123
54. Shi H, Liu F, Yang L, Han E (2008) Prog Org Coat 62:359–368
55. Ornaghi HL Jr, Moraes AGO, Poletto M, Zattera AJ, Amico SC (2016) Cellul Chem Technol 50:15–22
56. Kusior A, Banas J, Trenczek-Zajak A, Zubrzycka P, Micek-ilnicka A, Radecka M (2018) J Mol Struct 1157:327–336
57 Thompson JM (2018) Infrared spectroscopy. CRC Press, New York
58. Afzal A, Siddiqi HM (2011) Polym 52:1345–1355
59. de Almeida SFM, Nogueira NZS (1994) Compos Struct 28:139–148
60. Alamri H et al (2018) J Colloid Interface Sci 513:349–356
61. Kocijan A, Conradi M, Hočevar M (2019) Mater 12:1877
62. Ali F, Waseem M, Khurshid R, Afzal A (2020) Prog Org Coat 146:105726
63. Hamidi YK, Aktas L, Altan MC (2005) Compos Sci Technol 65:1306–1320
64. Salvatori D, Caglar B, Teixido H, Michaud V (2018) Compos Part A Appl Sci Manuf 108:41–52
65. Han KK, Lee CW, Rice BP (2000) Compos Sci Technol 60:2435–2441
66. Monticeli FM, Vidal DCSM, Shiino MY, Voorwald HJC, Cioffi MOH (2019) Polym Eng Sci 59:1215–1222
67. Ornaghi HL Jr, Monticelli FM, Neves RM, Zattera AJ, Cioffi MOH, Voorwald HJC (2020) Compos Commun 19:210–219
68. Ahad NA, Ahmad SH, Zain NM (2014) Adv Mater Res 879:107–111
69. Li S, Chen D, Gao C, Yuan Y, Wang H, Liu X, Hu B, Ma J, Liu M, Wu Z (2020) Compos Sci Technol 198:108292
70. Johnsen BB, Kinloch AJ, Mohammed RD, Taylor AC, Sprenger S (2007) Polym 48(2):530–541
71. Liang YL, Pearson RA (2009) Polym 50(20):4895–4905
72. Zhang H, Zhang Z, Fredrich K, Eger C (2006) Acta Mater 54(7):1833–1842
73. Li S, Wang H, Liu M, Peng C, Wu Z (2019) J Appl Polym Sci 136(2):46930
74. Yao D, Peng N, Zheng Y (2018) Compos Sci Technol 167:234–242
75. Dittanet P, Pearson RA (2012) Polym 53(9):1890–1905
76. Mohit H, Selvan VAM (2019) Iranian Polym J 28:823–837
77. Kothmann MH, Zeiler R, Anda AR, Bruckner A, Altstadt V (2015) Polym 60:157–163
78. Oladele IO, Ibrahim IO, Adediran AA, Akinwekomi AD, Adetula YV, Olayanju TMA (2020) Results Mater 5:100053
79. Bulut M (2017) Compos Part B Eng 122:71–78
80. Mohit H, Selvan VAM (2020) Polym Compos 41:1878–1899
81. Anidha S, Latha N, Muthukumar M (2020) J Mater Res Technol 9:7947–7954
82. Zheng W, Chen WG, Zhao Q, Ren SX, Fu YQ (2019) Polym 163:171–177
83. Papageorgiou DG, Kinloch IA, Young RJ (2017) Prog Mater Sci 90:75–127
84. Levchik SV, Camino G, Costa L, Luda MP (1996) Polym Degrad Stabil 54(2–3):317–322
85. Grassie N, Guy MI, Tennent NH (1986) Polym Degrad Stabil 14(2):125–137
86. Wang JS, Wnag DY, Liu Y, Ge XG, Wang YZ (2008) J Appl Polym Sci 108(4):2644–2653
87 Bai W, Lin J (2011) Prog Org Coat 71:43–47